Investigation into the Formation and Adhesion of Cyclopentane Hydrates on Mechanically-Robust Vapor-Deposited Polymeric Coatings

Hossein Sojoudi,[§,¶] Matthew R. Walsh,[#] Karen K. Gleason,[§] and Gareth H. McKinley[¶]**

[§]Department of Chemical Engineering, Massachusetts Institute of Technology, 77 Massachusetts Avenue, Cambridge, MA 02139, United States

[¶]Department of Mechanical Engineering, Massachusetts Institute of Technology, 77 Massachusetts Avenue, Cambridge, MA 02139, United States

[#]Chevron Energy Technology Company, Flow Assurance, 1200 Smith St, Houston, TX, 77002, United States

ABSTRACT

Blockage of pipelines by formation and accumulation of clathrate hydrates of natural gasses (also called gas hydrates) can compromise project safety and economics in oil and gas operations, particularly at high pressures and low temperatures such as those found in subsea or arctic environments. Cyclopentane (CyC5) hydrate has attracted interest as a model system for studying natural gas hydrates, because CyC5, like typical natural gas hydrate formers, is almost fully immiscible in water; and thus CyC5 hydrate formation is governed not only by thermodynamic phase considerations but also kinetic factors such as hydrocarbon/water interfacial area and mass & heat transfer, as for natural gas hydrates. We present a macro-scale investigation of the formation and adhesion strength of CyC5 hydrate deposits on bilayer polymer coatings with a range of wettabilities. The polymeric bilayer coatings are developed using initiated chemical vapor deposition (iCVD) of a mechanically-robust and

densely-cross-linked polymeric base layer (poly-divinyl benzene or pDVB) that is capped with a covalently-attached thin hydrate-phobic fluorine-rich top layer (poly-perfluorodecylacrylate or pPFDA). The CyC5 hydrates are formed from CyC5-in-water emulsions, and differential scanning calorimetry (DSC) is used to confirm the thermal dissociation properties of the solid hydrate deposits. We also investigate the adhesion of the CyC5 hydrate deposits on bare and bilayer polymer-coated silicon and steel substrates. Goniometric measurements with drops of CyC5-in-water emulsions on the coated steel substrates exhibit advancing contact angles of 148.3º ± 4.5º and receding contact angles of 142.5º ± 9.8º, indicating the strongly emulsion-repelling nature of the iCVD coatings. The adhesion strength of the CyC5 hydrate deposits reduced from 220±45 kPa on rough steel substrates to 20±17 kPa on the polymer-coated steel substrates. The measured strength of CyC5 hydrate adhesion is found to correlate very well with the work of adhesion between the emulsion droplets used to form the CyC5 hydrate and the underlying substrates.

INTRODUCTION

Clathrate hydrates are crystalline solids resembling ice in which a lattice of space-filling cage-like cavities is made up of hydrogen-bonded water molecules, with the cavities filled by guest molecules stabilizing the lattice structure.[1] The small guest molecules might be hydrocarbons (e.g., methane, ethane, propane), other gases (e.g., carbon dioxide, hydrogen) or liquid (e.g., certain alcohols, tetrahydrofuran, cyclopentane).[2-4] Blockage of oil and gas pipelines via the formation and accumulation of clathrate hydrates is a major concern for the oil and gas industry.[5] Hydrates may also form naturally in oceanic sediments or sediments under the permafrost, where thermodynamic conditions such as high pressures and low temperatures exist.[6-7]

There are active methods to prevent the formation and agglomeration of hydrate inside oil and gas pipelines including external heating of the pipelines,[5, 8] addition of water miscible

alcohols and glycols such as methanol or ethylene glycol to shift the thermodynamic equilibrium away from typical pipeline conditions,[9] and the use of low-dosage kinetic inhibitors or anti-agglomerates to reduce the rate of nucleation and growth of hydrates, or to prevent the agglomeration of hydrate particles into larger structures which increase the risk of blockage.[4, 10] Gas hydrate blockages pose an unresolved flow assurance challenge for hydrocarbon production with high watercuts because hydrate inhibition with thermodynamic inhibitors, such as methanol, often becomes economically and logistically unpractical.[11] Production from some oil and gas wells can be prematurely terminated as a result of risks of hydrate blockages because the extent of subcooling in deepwater production is generally too high for kinetic hydrate inhibitors to be effective, and it is commonly believed that anti-agglomerate hydrate inhibitors are not reliably effective (at economically feasible dosages) at watercuts higher than 50-60%. [4-5, 8-11] Therefore, passive methods such as surface modifications of pipeline inner walls are of interest for two reasons; firstly in order to minimize nucleation and/or deposition of hydrates on the pipeline wall, and secondly, in the case of wall formation or deposition to reduce the hydrate adhesion strength.[12]

In order to reduce the adhesion of ice to underlying substrates, we have recently developed durable and mechanically-robust bilayer polymer coatings which are covalently bonded to silicon and steel substrates through an in-situ grafting mechanism using the initiated chemical vapor deposition (iCVD) technique.[13] iCVD is a unique deposition technique that enables grafting of polymers to the underlying substrates. This enhances the adhesion of the coating and increases its durability against abrasion, erosion, and delamination.[14-16] Unlike traditional polymer deposition techniques such as spin-coating, dip coating or ink-jet printing, iCVD provides routes to (i) deposit polymer coatings which are graded in composition from the substrate up, (ii) deposit copolymers which do not have common solvents, and (iii) create multilayered polymer structures which are covalently bonded at their interface.[17-18] The conformal nature of the iCVD technique also enables the

deposition of polymeric thin films onto typical engineering surfaces that have appreciable surface roughness or nanostructured topography. Our cross-linked bilayer polymeric networks exhibit enhanced mechanical properties (e.g., elastic modulus and hardness) when compared to other coatings developed using traditional iCVD polymerization, making them more suitable for application in harsh environments, and thus perhaps in oil and gas pipelines for flow assurance strategies.[13]

At temperatures of industrial interest, hydrates of typical natural gasses are only thermodynamically stable at elevated pressures; thus, identifying suitable guest molecules which form hydrates at ambient pressure and moderate temperatures (e.g. above the ice point) are attractive as natural gas hydrate analogs for experimental investigations, due to the advantages in ease of experimental access, visualization, cost, and safety inherent in ambient-pressure experiments. Commonly-used ambient-pressure hydrate formers include tetrahydrofuran (THF) and cyclopentane (CyC5). We recently studied the formation and adhesion of THF hydrates on mechanically-robust bilayer iCVD polymer films and extended the application of such polymer coatings into the area of durable hydrate-phobic surfaces.[19] This application leveraged the scientific understanding of hydrophobic and icephobic surfaces; specifically, the strong linear correlation between the practical work of adhesion of a single-phase liquid droplet placed on the substrate and the measured adhesion strength of the solid deposit that is subsequently formed from this liquid.

However, because THF is miscible in water, the hydrate formation mechanism may be different than for hydrates of immiscible hydrocarbon/water mixtures, such as those found in oil and gas pipelines. In the present work we investigate the formation and adhesion of CyC5 hydrates to various surfaces. Cyclopentane is a hydrate former which is immiscible with water, and thus CyC5 hydrate formation is governed by the interfacial surface area of the water/guest molecule mixture, and by interfacial transport resistances, as is the case for natural gas hydrates. Studies of the formation mechanism and adhesion of CyC5 hydrates to potential

hydrate-phobic surfaces therefore more closely mimics the behavior of natural gas hydrates than does THF hydrate. At ambient conditions, CyC5 hydrate has a melting and dissociation temperature of approximately 7.7 °C and (analogous to the miscible case of THF in water) CyC5 forms a structure II hydrate with water at a molar composition ratio of H_2O:CyC5 equal to 17:1.

Crystallization, growth, and aggregation of CyC5 hydrate particles have been investigated in a series of studies by Sloan and coworkers.[4, 6, 9, 20-25] They formed CyC5 hydrate particles by freezing water droplets inside a bath of CyC5 and then brought them into contact with either similarly-formed CyC5 hydrate particles or various solid surfaces.[26-28] They used a micro-mechanical adhesion apparatus to measure the adhesion force between previously-formed hydrate particles,[22, 26] and/or hydrate and ice particles, with and without the presence of another liquid (e.g. crude oil).[27-28] The effects of contact force, contact time, and subcooling temperature were investigated in these studies.[22, 25-28] Hun et al. also studied the interaction between hydrate particles and water in a temperature-controlled hydrocarbon environment utilizing an apparatus fabricated with a microbalance and z-axis stage.[29-30] Both groups explained the trends observed in the measured adhesion forces in terms of a capillary bridge formed between the contacting hydrate particles and/or hydrate particles and liquid droplets. More recently, Aspenes et al. studied the adhesion forces between hydrate particles and a number of solid surfaces with various surface energies in the presence of water and/or other petroleum acids in an oil phase. They found that the adhesion force between the hydrate particles and the solid surfaces increases more than 10 times when the solid surfaces are preferentially water-wet.[25]

Several other groups have investigated the bulk formation of CyC5 hydrates from a CyC5-in-water emulsion.[31-33] Morris and coworkers have performed calorimetric investigation of CyC5 hydrates formed from an emulsion, providing insight into the mechanism of CyC5 hydrate nucleation and growth.[31-33] They have experimentally

investigated heterogeneous nucleation of CyC5 hydrates by ice in conjunction with rheological measurements of the properties of hydrate-forming emulsions as the hydrate phase nucleates and grows. Nakajima et al. reported the formation of hydrate from CyC5-in-water emulsions as a potential thermal energy storage media for air-conditioning systems.[34] Sefidroodi et al. investigated the strength and the source of the so-called "memory effect" in the formation of CyC5 hydrates. They observed that if only a few degrees of superheating above the CyC5 hydrate equilibrium dissociation temperature (7.7 °C) are imposed on a sample then formation of hydrates occurs much more rapidly during subsequent cooling to 0.0 °C, as compared to the case when hydrates are formed from the liquid for the first time.[35]

Despite these extensive studies on the nucleation and growth of CyC5 hydrates both in particulate and bulk forms, there is a lack of data on their formation and bulk adhesion on engineering substrates of various surface energies. While previously-formed hydrate particles may deposit on existing water-coated or hydrate-coated pipelines, in many other applications, hydrate may form directly on bare steel pipeline walls and deposit to form a film.[25] In this situation, and in the absence of external remediation, the deposited hydrate film can grow into a bulk hydrate and the flow path through the pipe becomes obstructed. Brown et al. have used laser induced fluorescence (LIF) for observing CyC5 hydrate formation and shown that, in the absence of mixing, hydrate film formation can be observed..[36] However, to understand the impact of hydrate crystallization on the resulting adhesion strength, there is a need to study the in-situ formation of bulk CyC5 hydrates on engineering surfaces and investigate the effect of surface energy on the resulting adhesion strength. In the present study, both the bulk formation and subsequent adhesion of CyC5 hydrates to bare and iCVD polymer-coated silicon and steel surfaces are investigated. A CyC5-in-water emulsion is used to form CyC5 hydrates. Differential scanning calorimetry measurements are performed to ensure the presence of hydrates by examining the temperature and latent heat of the CyC5 hydrate dissociation. The strength of CyC5 hydrate adhesion is reduced by a factor of ten when the

bare silicon and steel substrates are coated with the iCVD bilayer polymer coatings. We also measure the advancing and receding contact angle of droplets of a CyC5-in-water emulsion deposited on bare and polymer-coated substrates using goniometry. We find a strong linear correlation between the measured strength of CyC5 hydrate adhesion and the practical work of adhesion between the emulsion droplets and the underlying substrates. The present study of hydrate formation and systematic control of its adhesion to rigid metallic surfaces may be useful in addressing the issue of flow assurance in petroleum pipelines.

We have recently reported the design and deposition of iCVD bilayer polymeric networks with enhanced mechanical properties and improved adhesion to underlying substrates by promoting chemical bonds across the substrate-polymer interface through a linker-free grafting mechanism.[13] The bilayer stack consisted of a thick, highly cross-linked, mechanically-robust and densely cross-linked poly-divinyl benzene (pDVB) base layer with enhanced mechanical properties (e.g. a higher elastic modulus and hardness) capped with a covalently-attached thin hydrophobic fluorine-rich top layer, poly(perfluorodecylacrylate) (pPFDA). When deposited on steel substrates, the resulting bilayer film displayed high elastic modulus and hardness (E=19.1±1.2 GPa and H = 479.0±7.0 MPa, respectively), excellent Cassie state hydrophobicity (advancing water contact angle (WCA) on steel, θ_A^w=154.2º ± 2.2º, and receding WCA on steel, θ_R^w=150.3º ± 1.6º), and strong adhesion to the underlying substrates (i.e. the films did not delaminate during nanoscratch tests performed at 5 mN normal loads). Finally, these bilayer coatings reduced the adhesion strength of pure ice and THF-hydrates by more than six-fold and ten-fold, respectively.[19, 37]

RESULTS AND DISCUSSION

Our previous work extensively describes the deposition and linker-free grafting mechanism of bilayer CVD polymers.[13] Thus, we only provide a brief summary in this section.

First, treatment with solvents (e.g. acetone and methanol) cleaned the surfaces of the chosen growth substrates (e.g. silicon wafers or steel coupons) and exposure to oxygen plasma enhanced the surface concentration of hydroxyl species. Then, the substrates were placed in a low pressure iCVD reactor. The subsequent grafting and synthesis proceed in three steps, all performed sequentially in the iCVD chamber without breaking vacuum: 1) in-situ linker-free grafting, 2) deposition and growth of a mechanically-robust cross-linked hydrocarbon network, and 3) deposition of the top fluoropolymer layer.

For the linker-free grafting, a vapor of *tert*-butyl peroxide (TBPO) initiator was exposed to hot filament arrays kept at T_f = 310ºC to produce methyl radicals[38-39] which can abstract hydrogen from the hydroxyl groups on the plasma-treated substrate (which was maintained at T_s = 20ºC). This resulted in activated radical sites on the surface [38] which directly reacted with the vinyl monomers to be introduced subsequently, to produce covalent bonds from the substrate to the growing organic layer.

Next, divinylbenzene (DVB) monomer flowed to the reactor without filament heating (T_f = 25ºC) while the substrate was kept at T_s = 20ºC. The initial reaction with the activated surface sites resulted in direct grafting of the monomer to the substrate while retaining a free electron for subsequent vinyl polymerization.

For polymerization of a mechanically-robust layer in the second step, DVB, N_2, and TBPO flowed simultaneously to the low pressure reactor with the filament and the substrate temperatures of T_f = 250ºC and T_s = 30ºC, respectively.[40] This resulted in deposition of a densely cross-linked DVB polymer (pDVB) network with the desired thickness (in the range of 200 nm – 1 μm).

The third and final step is to grow a top surface layer displaying both low surface energy and the desired hydrate-phobicity. For this, poly-perfluorodecylacrylate, poly-(1H, 1H, 2H, 2H-perfluorodecylacrylate) (pPFDA) was introduced into the reactor to deposit a thin top layer of fluorine-rich polymer. We have reported results with two different thickness of

pPFDA (either 10 or 40 nm thick) on both flat silicon (henceforth denoted as 'BL (10 nm) on Si' and 'BL (40 nm) on Si' respectively) and rough steel substrates (henceforth denoted as 'BL (10 nm) on steel' and 'BL (40 nm) on steel'). We have shown that while a thick pPFDA film (40 nm) can ensure a more complete coverage of the bilayer film, the presence of the densely cross-linked pDVB network underneath a very thin 10 nm pPFDA film can prevent inward reorientation of fluorine groups in the pPFDA top layer when it is exposed to water, resulting in lower water contact angle hysteresis (θ_A^w- θ_R^w).[18] A summary of water contact angle (WCA) measurements on BL (10 nm) and BL (40 nm) coatings deposited on flat silicon and rough steel substrates is presented in Table 1.

Fourier transform infrared spectroscopy (FTIR) and X-ray photoelectron spectroscopy were performed on the bilayer polymer networks and confirmed successful deposition of both pPFDA and pDVB components through the presence of bands corresponding to carbonyl, carbon-fluorine bonds, and phenyl groups in the FTIR spectra.[13] The properties of the BL films can be summarized as follows. Optical profilometer measurement gave root mean square (RMS) roughness value of R_q = 34.2±5.2 nm and R_q =28.3±3.8 nm for BL (40 nm) on Si and BL (10 nm) on Si, respectively.[13] In addition, an RMS roughness value of R_q = 132.5±17.4 nm and R_q = 120.3±22.0 nm were obtained from measurements performed on BL (10 nm) on steel and BL (40 nm) on steel samples, respectively. The increase in the RMS roughness value of the bilayer polymer film when deposited on the steel coupons (as compared to the value measured on the silicon wafer) comes from the roughness of the underlying steel substrate. The elastic moduli and hardnesses of the bilayer films were obtained from nanoindentation measurements giving values (on silicon substrates) of E = 19.1±1.2 GPa and H = 479.0±7.0 MPa for the 40 nm bilayer films and E = 18.1±1.0 GPa and H = 463.0±4.5 MPa on the thinner 10 nm films. It is important to note that the elastic modulus and hardness are controlled primarily by the densely cross-linked pDVB network and not by the thin top layer pPFDA film or the underlying substrate; therefore, both the BL (40 nm) and

the BL (10 nm) films showed comparable elastic modulus and hardness values on silicon and steel substrates.[13]

Formation of CyC5-in-Water Emulsion. Emulsions of CyC5 (Sigma-Aldrich, ≥99%) and deionized water, in which 4% Tween 85 (Sigma-Aldrich) was first dissolved to serve as an emulsifier, were prepared in sealed glass vials by 30 minutes of ultrasonication (Aquasonic 150D, VWR at a power level of 9).[41] The water-to-CyC5 molar ratio in every sample was held fixed at approximately 17:1, in agreement with the stoichiometric host-to-guest molar ratio in a structure II hydrate with full occupation of its $5^{12}6^4$ cages by guest molecules.[34] A freshly prepared emulsion sample was transferred into a rectangular capillary placed on a glass slide for imaging under the microscope. Figure 1 shows representative photomicrographs of the as-made emulsion and again 4 hr after preparation. The glass vials were gently inverted a few times before sampling for these images. The Tween 85 surfactant helps stabilize the emulsion against rapid coalescence and the droplet size distribution changes slowly over 4 hours (see Table 2). The droplet diameter, averaged over 10 independent samples, changed from 8.4 ± 3.8 μm to 5.8 ± 3.4 μm after 4hr, which provides sufficient stability of the emulsions to perform hydrate formation experiments by extended cooling. The large standard deviations measured arise from both sample-to-sample variations as well as a slow change in the droplet size. The emulsion was also found to be relatively stable against rapid coalescence when maintained at -15 °C as well.

Formation of CyC5 Hydrates. To study the formation of CyC5 hydrates, approximately 4 ml of the stabilized CyC5-in-water emulsion was poured into a glass cuvette and placed on a Peltier cold plate inside a custom-built transparent acrylic box. A steady nitrogen flow was maintained inside the acrylic box to ensure low humidity and to prevent frost formation. The temperature of the cold plate decreased to -15 °C within several minutes and was maintained for 30 minutes to ensure the formation of ice/hydrate. Visual observation of the formation of CyC5 hydrates was performed by a digital camera with macro lens (EOS 7D).

Figure 2 shows snapshots obtained by viewing the sample through the transparent acrylic box and glass cuvette (see Supporting Information for a video of hydrate formation). Figure 2a shows the stabilized emulsion of CyC5 droplets in water before cooling to low temperature. Figures 2b, c, and d show the nucleation and growth of the ice/hydrate phase while the substrate temperature was held at -15 °C. As time passes and thermal energy is removed from the system by the Peltier plate, the sample in the cuvette mostly turns into a solid. The temperature of the cold plate was then increased incrementally (0.5 °C/min) until it reached 0.0 °C (figure 2e) and was maintained at this temperature for 5 minutes to allow melting of any ice that may be formed. Figure 2f shows that upon warming to 0.0 °C, ice was observed to melt from the periphery of the cuvette leaving a core hydrate. To ensure the entire sample experiences a temperature above the equilibrium ice melting point (and to melt any residual ice), the temperature was then increased to 2 °C (figure 2g). Hydrate formation occurs simultaneously with ice melting as soon as there is free water at the oil/water interface of the frozen CyC5 slurry. CyC5 hydrate formation could be visually observed to start when the CyC5-in-water emulsion became cloudy and dark. The dark and cloudy appearance in the solid inside the cuvette is indicative of formation of the hydrate. Finally, the temperature was increased gradually (in approximately 0.3 °C/min increments) until it reached 5 °C (figure h) to allow further ice melting which provides free water at the interface with CyC5. The temperature was then maintained at this temperature for 60 minutes (figure 2i) to ensure melting of ice and the equilibration of the microstructure. Any remaining solid in the cuvette at 5 °C must be a CyC5 hydrate (T_M = 7.7 °C). The ice, which melts away during warming, provides free water and thus the core slushy remnants act as sites for reforming hydrates while stabilizing the temperature (e.g. at 5 °C) just below the equilibrium hydrate forming point.

The cyclopentane hydrate formation process is an interfacially-mediated phenomenon that proceeds with a rate that depends on the availability of interfacial area between the water and the hydrate former (CyC5). Using the protocol described above CyC5 hydrates can be

prepared without continuous agitation of the emulsion. The rapid initial cooling of the emulsion results in freezing of the emulsion droplets before coalescence. When the temperature is raised just above the ice melting point, the high contact area between the continuous phase liquid water and the dispersed oil drops promotes nucleation and growth of the cyclopentane hydrate. Zhang et al.[41] and Karanjkar et al.[31] also observed the formation of hydrate without continuous agitation in their DSC studies of hydrate formation. In our work, the interfacial area between the water and the CyC5 is higher than previous literature reports due to the small size of the CyC5 droplets (~ 5-10 μm in diameter).[31] Considering the microscopic size of the CyC5 droplets it was not possible to image through the bulk hydrate due to light scattering effects. For this reason, we rely on direct visual observation of hydrate formation to show the interface between the hydrate phase and the emulsion. Blank negative control tests with no CyC5 were carried out intermittently to check that no ice/hydrate formed from samples containing only water that underwent the identical thermal cycling procedure.

Differential Scanning Calorimetry Measurements. After the hydrate formation process was finished, a small quantity of the formed hydrate was sampled from the cuvette and then subjected, after overnight storage in a refrigerator at approximately -10 °C, to a measurement of the heat of hydrate dissociation by differential scanning calorimetry (hereafter abbreviated as DSC). Figure 3a and b show pictures taken from the CyC5 hydrate inside a cuvette and a small piece sampled for the DSC measurements, respectively. The test cell used for the DSC measurements was made of aluminum and sealed with an aluminum cap. A Perkin Elmer Pyris 1 DSC calibrated with 99.99% standard indium was used for calorimetric studies. The working principle is based on differential measurement of the temperature of a sample and the reference; the necessary heat flow required to achieve a zero difference between the two is recorded as an output.[31] Prior to the measurement of the hydrate samples, the latent heat and the temperature of fusion of a non-hydrate containing (100% water-ice system) was measured for use as a comparative standard for evaluating the latent heat and the dissociation

temperature of an ice/hydrate system from the relevant DSC data. The Experimental Section details the test procedure.

Figure 3c compares the heat flow curves in a DSC trace of the hydrate and the non-hydrate/pure ice systems for the same temperature protocol. Since, inevitably, some fraction of the sample in both the hydrate-containing and non-hydrate system was melted during the procedure of sample loading into the test cell, each sample was first subcooled in order to freeze any residual free water. The temperature was decreased from 15 °C to -20 °C and then brought back to 15 °C at a fixed ramp rate of 1 °C/min in each direction. DSC data shows an exothermic peak during the cooling ramp in both systems, due to freezing of free water and the formation of an ice shell. Karanjkar et al. have observed a single exothermic peak during cooling based on an energy balance and concluded that there is only ice formation in this step.[31] Fouconnier et al. observed a similar single exothermic peak during cooling, and they utilized X-ray diffraction coupled with DSC to separate ice formation, ice melting, hydrate formation, and hydrate dissociation peaks.[42] The ice formation exothermic peak is around -15 °C for both systems. This is close to the ice formation peak reported by Karanjkar et al.[31] (~ -20 °C) but significantly higher than the ice nucleation temperature of -38 °C reported by Clausse.[43] In addition, an asymmetry was observed in the ice formation peak which is in contrast to Clausse.[43] Karanjkar et al.[31] have argued that the disagreement with Clausse's measurements might be due to some crowding of droplets due to gravitational settling of water drops.[31, 43] Zhang et al. also observed an exothermic peak around -15 °C which is believed to be related to the heterogeneous nucleation of ice.[41] Once ice nucleation occurs, they speculated that the water drops may undergo a rapid phase change with energy release characteristics similar to that observed for bulk water.

Upon subsequent heating there is an endothermic peak observed in both systems near 0.2 °C relevant to heat uptake as a result of ice melting. In the hydrate system, during heating an additional endothermic peak corresponding to the hydrate dissociation was observed in the

range of 6-7 °C. This is close to the phase-equilibrium temperature (T_{eq}) of CyC5 hydrate that has been previously reported in the literature (6.6 °C $\leq T_{eq} \leq$ 7.7 °C).[31, 34]

The area under the endothermic peaks measured during heating provides the latent heat associated with ice melting and hydrate dissociation. From the non-hydrate system, the latent heat of fusion of water ice was found to be h_w = 334 kJ/kg which is very close to the reference value of the heat of fusion for ice at atmospheric pressure, h_w = 333.427 kJ/kg.[44] This can be used as the standard for the evaluation of the heat of hydrate dissociation from the DSC data. For the hydrate system, the latent heat of CyC5 hydrate dissociation was measured to be 117.4 kJ/kg (see Experimental Section for details). Nakajima et al. have reported that the effective heat of dissociation of CyC5 hydrate masses with no dewatering procedure range from 41 to 220 kJ/kg.[34] They have also shown a tendency for an asymptotic increase in the heat of hydrate dissociation with an increase in the surfactant concentration.[34] In addition, a dewatering procedure has shown promise in effectively increasing the heat of hydrate dissociation.[34, 41]

Wettability of Bilayer iCVD Polymer-Coated Surfaces by Emulsion Droplets. The CyC5-in-water emulsion was prepared in a manner similar to the protocol explained in Section 2.1 and its effective interfacial tension and impact on wettability of surfaces (iCVD bilayer polymer-coated and bare substrates) were studied. The effective interfacial tension of the CyC5-in-water emulsion was measured through the pendant drop method.[45] Measurements were performed on the as-made emulsion and again 4hr after its preparation. Following the same procedure as used for obtaining the microphotograph images, the glass vials containing the emulsion were inverted gently a few times prior to sampling for the goniometry measurements. The effective surface tension for the emulsion was found to be 59.3±1.8 mN/m, averaged from measurements of ten droplets of as-made emulsion and samples taken 4hr after emulsification. The surface tension of distilled water (71.0±1.0 mN/m) and CyC5 (24.2±0.8 mN/m) were also measured independently and used for confirming the accuracy of

the tensiometry measurements. Given the high molar ratio of water/CyC5 (17:1) and the fact that the emulsion consists of discrete cyclopentane droplets in a continous water phase with a small amount of additional surfactant; it is to be expected that the effective interfacial tension of the emulsion is signifcantly higher than the surface tension of pure CyC5 and is closer to the surface tension of water.[5]

The wettability of the bare substrates and the iCVD polymer bilayer coatings by the emulsion was also investigated. Contact angle measurements provide a useful tool for probing interfacial interactions between a solid and a liquid. The wettability of a surface by a pure liquid or a mixture can be enhanced by either reducing the liquid surface tension or by increasing the substrate surface energy. In Table 1 and Figure 4 we show the measured advancing and receding contact angles of CyC5-in-water emulsion droplets on bare and coated silicon and steel substrates. In Fig 4(b) we show representative emulsion droplet images captured during the contact angle measurements on bare Si (top), BL (40 nm) on Si (middle), and BL (10 nm) on Si (bottom). The bare Si substrate is hydrophilic and exhibits both low advancing (32.5º ± 2.1º) and receding (9.1º ± 1.7º) contact angle values for the emulsion drop. The linker-free grafted bilayer pDVB/pPFDA polymer with a top pPFDA thickness of ~ 40 nm on Si (BL (40 nm) on Si) resulted in much higher advancing (θ_A=135.7º ± 6.7º) and receding (θ_R=122.1º ± 7.5º) contact angles for the emulsion droplets due to the high density of fluorine-containing groups in the pPFDA layer. Corresponding values for water contact angles (WCA) on this substrate are even higher (θ_A^w=149.1º ± 1.9º and θ_R^w=132.0º ± 7.8º) which is consistent with the higher surface tension of a water droplet when compared to CyC5-in-water emulsion.[13] Small variations in the measured contact angles might be due to local differences in the surface morphology or crystallinity of the top pPFDA layer which can arise from variations in the polymer deposition.[15, 17] The 40 nm pDVB/pPFDA bilayer was also deposited on the steel surface and resulted in advancing and receding contact angles for the emulsion droplets of θ_A=138.5º ± 7.5º and θ_R=125.2º ± 10.1º,

respectively. The increase in the measured advancing and receding contact angles for the emulsion droplets over the values measured on the silicon substrate is due to the enhanced surface roughness of the linker-grafted polymer film that originates from the underlying rough steel substrate.[46]

The linker-free grafted bilayer film (pDVB/pPFDA) with a thinner pPFDA top layer (~ 10 nm) was also deposited on the silicon substrate (denoted 'BL (10 nm) on Si') and this resulted in an increase in both the advancing (θ_A=147.6º ± 5.4º) and the receding (θ_R=140.5º ± 6.6º) contact angles for the CyC5 emulsion droplets. We have observed similar trends in the advancing and receding contact angles for water droplets on 10 nm thick pPFDA layer as well ($\theta_A^w = 152.0° \pm 1.0°$ and θ_R^w=145.0º ± 1.8º).[13] Similar to the trends reported above for the thicker pPFDA layer (40 nm), a slight increase in the contact angles for the emulsion droplets on the thin bilayer film deposited on steel substrates (denoted 'BL (10 nm) on steel') was observed (θ_A=148.3º ± 4.5º and θ_R=142.5º ± 9.8º), when compared to the polymer films deposited on Si substrates.

In summary, a decrease in the contact angle hysteresis ($\theta_A - \theta_R$) for droplets of water and for the CyC5 emulsion is observed when the pPFDA layer thickness is decreased to ~ 10 nm on both substrates (Si and steel). We have shown in our previous studies that the presence of the densely-cross-linked and rigid pDVB network underneath an ultrathin pPFDA film (~ 10 nm) can prevent inward reorientation of the fluorine groups in the pPFDA layer when exposed to partially-wetting liquids and this results in the lower contact angle hysteresis that is observed macroscopically.[18] It is to be noted that all of the substrates are wetted by pure CyC5 droplets due to the very low surface tension of cyclopentane. Overall, the thinner bilayer coating (10 nm) shows enhanced repellency to an emulsion of CyC5-in-water when compared to a thicker bilayer (40 nm) on both substrates and this suggests that the latter coating is likely to perform better at reducing the strength of CyC5 hydrate adhesion.

CyC5 Hydrate Formation and Strength of Its Adhesion to Surfaces. Next, we study the formation of CyC5 hydrates and the strength of their adhesion to bare surfaces and polymer-coated substrates with two different top layer thicknesses (BL (10 nm) and BL (40 nm)). A custom-built adhesion testing apparatus housed inside a nitrogen-containing glove box was used for this purpose.[13] The CyC5-in-water emulsion was prepared similar to the method explained earlier, poured into glass cuvettes, and then underwent the same thermal conditioning process described in Section 2.2 to ensure formation of CyC5 hydrates on the substrates inside the cuvettes.[12] Care was taken to minimize air exposure of the emulsion, and the time elapsed between its preparation and pouring into cuvettes for the strength of adhesion measurements was also kept to a minimum (less than a minute) in order to minimize CyC5 evaporation and emulsion droplet coalescence.

The lateral force required to fracture the frozen cuvettes from the substrate was recorded and converted into a measure of the shear strength of CyC5 hydrate slurry adhesion by dividing over the cuvette area. The measurements were performed on twenty samples of each type and then ensemble averaged. Sample-to-sample variations in the measured adhesion strengths are large due to the dominant role of local flaws in adhesive failure tests and local variations in the nature of the CyC5 hydrate formed at the interface with the substrate. Another factor contributing to variations in the data might be possible differences in hydrate numbers as some cages in the hydrate structures formed might not be occupied with CyC5 guest molecules.[47]

The strength of CyC5 hydrate adhesion on bare silicon substrates was measured to be 207±65 kPa, whereas on the bilayer polymer coatings, BL (40 nm) on Si and BL (10 nm) on Si, it was reduced to 36±14 kPa and 22±12 kPa, respectively. Steel substrates coated with a linker-free bilayer of the perfluorinated pPFDA polymer (BL (10 nm) on steel) resulted in CyC5 hydrate adhesion strength of 20±17 kPa, which is a ten-fold reduction when compared to the corresponding adhesion values measured on bare steel substrate (220 ± 45 kPa). There

is an enhanced reduction in the strength of CyC5 hydrate adhesion on the thinner BL (10 nm) when compared to the thicker BL (40 nm) on both substrates (Si and steel) which is consistent with the enhanced liquid repellency to CyC5-in-water emulsion droplets observed on both substrates for the thinner pPFDA film.

It may be conjectured that there is a difference between the actual temperature inside the cuvettes and the cold plate temperature. Therefore, to understand possible differences in the nature of the formed CyC5 hydrates and the strength of their adhesion to the different substrates, adhesion measurements were also carried out at cold plate temperatures of +2 °C and +4 °C. While Corak et al. have shown that the kinetics of hydrate formation at lower levels of subcooling are significantly slower than the kinetics at higher subcooling temperatures,[47] we find that the measured adhesion strength values are within the same range, indicating minimal impact, if any, of the subcooling temperature in this temperature range. This finding is in accord with Zhang's observation.[41]

Relation between Surface Wettability and the Strength of CyC5 Hydrate Adhesion. It has been shown that the wettability and motion of liquid droplets on surfaces involve two distinct kinematic processes: shear and tensile.[48-50] While shear deformation is related to sliding and/or roll-off of liquid droplets from surfaces (shear hydrophobicity), tensile deformations are more closely related to measurements of the pull-off force required to detach a droplet from a surface (tensile hydrophobicity). This latter quantity is related to the work of adhesion between a liquid droplet (e.g. a droplet of CyC5-in-water emulsion) and the underlying substrate and can be calculated from the Young-Dupré equation: [48-50]

$$W^{adh} = \gamma_{LV}(1 + cos\,\theta_R) \qquad (1)$$

where W^{adh} is the work of adhesion between a liquid droplet (e.g. a drop of CyC5-in-water emulsion) and the underlying substrate; γ_{LV} is the surface tension between the liquid (e.g. a drop of CyC5-in-water emulsion) and air; and θ_R is the receding contact angle of the CyC5-in-water emulsion droplet on a substrate.

A high receding contact angle of a CyC5-in-water droplet on a substrate corresponds to low pull-off forces under tensile (normal) loading conditions. To reflect the importance of tensile hydrophobicity, we present our results for the strength of CyC5 hydrate adhesion by plotting the measured values obtained from the adhesion apparatus vs. the work of adhesion between a liquid droplet (i.e. the CyC5-in-water emulsion) and a given substrate (either bare or polymer coated). Figure 4c shows that the average strength of CyC5 hydrate adhesion linearly reduces with decreases in the work of adhesion of an emulsion droplet placed on either substrate (with correlation coefficients R^2_{steel} = 0.98 and R^2_{Si} = 0.99). The trend observed in this data is consistent with our previously-observed trend in the strength of ice adhesion on icephobic coatings[13] and suggests that the adhesion strength of CyC5 hydrate on an underlying substrate correlates well with the work of adhesion of a CyC5-in-water emulsion droplet, from which the hydrate phase will subsequently nucleate and grow on the cooled substrate.

Overall, very good linear correlation between the measured hydrophobicity of CyC5-in-water emulsion droplets placed on the deposited polymer films and their corresponding hydrate-phobic behavior is observed. These results confirm that surfaces with stronger CyC5-in-water emulsion-repelling character are optimal for reducing the strength of CyC5 hydrate adhesion. The reduction in the strength of hydrate adhesion reported in this work is higher than those values reported elsewhere for soft fluorinated polymer coatings.[51-52] The high modulus and stiffness of the cross-linked polymer networks that are deposited by the iCVD process prevent surface remodeling when wetted and also provide greatly enhanced mechanical resistance to the wear and erosion processes that are characteristic of industrial applications. Future studies should investigate the repelling character of substrates to emulsion droplets on the microscale (corresponding to the length scale of individual droplets) and its relation to macroscopic goniometric measurements of emulsion droplets, as well as the

subsequent impact on the strength of macroscale cyclopentane hydrate adhesion to different rough textured substrates.

CONCLUSION

In conclusion, we have studied the formation and deposition of cyclopentane (CyC5) hydrates from subcooled CyC5-in-water emulsions and the adhesion of these hydrates to thin cross-linked fluorinated bilayer polymer coatings. The large CyC5/water interfacial area in the emulsions yield high rates of hydrate formation when the emulsion is cooled below the hydrate phase equilibrium temperature. Visual imaging allowed direct observation of hydrate formation and DSC measurements verified formation of the CyC5 hydrate and calculation of the heat of CyC5 hydrate dissociation. Contact angle measurements of emulsion droplets placed on the iCVD-coated surfaces revealed the emulsion-repelling nature of the mechanically-robust bilayer polymer films we have developed. The bilayer pDVB/pPFDA polymer coatings reduced the strength of CyC5 hydrate adhesion by up to ten-fold. We found a strong linear correlation between the measured strength of CyC5 hydrate adhesion and the practical work of adhesion calculated via the Young-Dupré equation for a droplet of CyC5-in-water emulsion that is placed on the underlying substrate. The results of this work suggest that the CyC5-in-water emulsion can be effectively used as a probe liquid for evaluating the adhesion strength of CyC5 hydrates on different coatings. The ten-fold reduction in hydrate adhesion on the cross-linked pDVB network capped with a very thin pPFDA coating offers a pathway forward for future passive and additive-free flow assurance applications in the oil and gas arena.

EXPERIMENTAL

iCVD Coatings. in-situ grafting and iCVD polymerizations were carried out in a custom-built cylindrical reactor (diameter 24.6 cm and height 3.8 cm), supporting an array of 14 parallel chromoalloy filaments (Goodfellow) suspended 2 cm from the stage.[15, 17] The reactor was

covered with a quartz top (2.5 cm thick) that allows real-time thickness monitoring by reflecting a 633 nm He-Ne laser source (JDS Uniphase) off the substrate/polymer and recording the interference signal intensity as a function of time. The reactor was pumped down by a mechanical Fomblin pump (Leybold, Trivac) and the pressure was monitored with a MKS capacitive gauge. The liquid monomers (1H, 1H, 2H, 2H-perfluorodecyl acrylate, PFDA, 97% Aldrich) and (divinylbenzene, DVB, 80% Aldrich) and the initiator (*tert*-butyl peroxide, TBPO, 98% Aldrich) were used as received without further purification. TBPO was kept at room temperature (T_f= 25ºC) and was delivered into the reactor through a mass flow controller (1479 MFC, MKS Instruments) at a constant flow rate of 3 sccm during grafting, and 3 sccm and 1 sccm in DVB and PFDA during polymerization, respectively. Methyl radicals were formed by heating the filaments to T_f = 310ºC during grafting using a DC power supply (Sorensen), whereas initiator radicals (TBO) were created by breaking only the labile peroxide bond of the TBPO at a filament temperature of T_f = 250ºC during polymerization. PFDA and DVB were vaporized in glass jars that were heated to 80ºC and 60ºC, respectively and then introduced to the reactor through needle valves at constant flow rates of 0.1 and 1 sccm, respectively. The substrate temperature was kept at T_s = 20ºC during grafting and 30ºC during polymerization (within ±1ºC) using a recirculating chiller/heater (NESLAB RTE-7). All of the temperatures were measured by K-type thermocouples (Omega Engineering). The working pressure was maintained at 800 mTorr during grafting and 650 mTorr and 300 mTorr in DVB and PFDA polymerization, respectively, using a throttle valve (MKS Instruments). Prior to in-situ grafting, silicon wafers (Wafer World Inc.) were first cleaned by sonication in acetone and isopropanol each for 5 minutes, followed by rinsing in DI water (>16 MΩ-cm). The surfaces were then treated with oxygen plasma for 10 minutes to provide further cleaning and to create surface hydroxyl groups prior to transfer into iCVD reactor.

DSC Measurements. A Perkin Elmer Pyris 1 DSC was used to determine the temperature and heat of dissociation of ice and hydrate. Temperature and heat calibration

were based on melting point and measurement of the enthalpy of fusion for 99.99% indium. This procedure was further checked using the measured melting temperature and heat of fusion of ice, corresponding more closely with the experimental temperature range. The temperature accuracy is estimated to be ± 0.1 °C. Prior to the measurements for the hydrate sample, a small piece of ice (15 mg) was placed inside an aluminum test cell (kept at low temperature inside an ice bucket) and sealed. The test cell was cooled to -20 °C at the rate of –1 °C/min to freeze any free water that might have formed around the ice during handling and placing inside the DSC. This can be confirmed by appearance of a small exothermic peak in the DSC data during the cooling process (Figure 3c dashed line). After keeping the test cell at -20 °C for a couple of minutes, the test cell was heated up to 15 °C at the rate of 1 °C/min. An endothermic peak at 0.2 °C was observed associated with ice melting. The quantity of heat transferred into the sample by water ice melting, denoted q_w, was evaluated by integrating the area under the endothermic peak, and was then divided by the known mass of the water ice (15 mg), which gives h_w=334.0 kJ/kg for the latent heat of fusion of water ice. Next, a small piece of CyC5 hydrate sample (stored in a temperature-controlled fridge at -10 °C and transferred inside an ice bucket for DSC measurements), was placed inside a sample holder similar to the method explained earlier, and underwent through the same process of cooling and heating. The mass of the empty cell was measured and subtracted from the mass of the cell filled with the hydrate (performed after finishing the experiment) to obtain the sample mass, m. During the heating, peaks due to the fusion of the ice and dissociation of the hydrate can be observed (Figure 3c, solid line). The quantity of heat transferred into the system to result in fusion of the ice, q_1, and dissociation of the cyclopentane hydrate, q_2, was calculated from the DSC data. The test cell contains both hydrate and ice, formed during the freezing of the free water. The mass of water, m_w, was obtained from the following relation:

$$m_w = q_1/h_w \qquad (2)$$

The mass of cyclopentane hydrate in the cell was obtained by subtracting the mass of free water, m_w, from the total mass, m:

$$m_h = m - m_w \qquad (3)$$

The latent heat of the hydrate dissociation, h_h, was then calculated using the following relation:

$$h_h = q_2/m_h \qquad (4)$$

Surface Tension and Contact Angle Measurements for CyC5-in-Water Emulsion. The surface tension of the CyC5-in-water emulsion and the advancing and receding contact angles were measured using a goniometer equipped with an automated dispenser (Model 500, ramé-hart). The effective surface tension of the stable CyC5/water emulsion was calculated using the pendant drop method.[45] Measurements were performed on the as-made emulsion and 4 hr after preparation. In both cases, the measurement was done rapidly after sampling the emulsion from sealed glass vials to minimize impact of air exposure on the cyclopentane droplets in the emulsion. The surface tension values were ensemble averaged from measurements on ten separate droplets. Advancing and receding contact angles were measured with the sessile drop method by depositing an emulsion droplet of 5 μL on the surface of interest and then increasing the volume by 0.15 μL increments until advancement in the liquid meniscus was observed, followed by then decreasing the drop volume by the same rate until receding motion was seen.[53] Advancing contact angles correspond to the maximum angles observed during the droplet growth, while receding contact angles were measured from the drop profile just before the interface receded. Each contact angle value was averaged from measurements using five emulsion droplets.

Strength of CyC5 Hydrate Adhesion Measurements. The strength of hydrate adhesion was measured using a custom-built set up whose details are described elsewhere.[51, 54] The bare substrates and polymer-coated samples (BL (10 nm) and BL (40 nm)) were cut into 1.5 cm × 1.5 cm pieces and clamped to a base plate. Then, glass cuvettes with a 1 cm × 1

cm cross section and approximately 90% filled with the CyC5-in-water emulsion were inverted on the substrates and clamped. Care was taken to remove any possible liquid residue on the substrate around the cuvettes. To form hydrates the samples underwent the same thermal conditioning explained in Section 2.2 using a Peltier plate (TECA Corporation, model LHP-800CP) in a low-humidity nitrogen atmosphere (humidity < 5%). After hydrate formation, the probe of a force transducer (Imada, model ZP-44), mounted on a single axis translation stage, was used to apply a progressively-increasing shear force to the cuvettes, and the maximum force required to fracture the crystal solid-substrate interface was recorded. The probe was located about 1.3 mm above the substrate surface to minimize torque on the hydrate sample. This distance was held constant for all samples with the same substrate type. The force measurement tests were performed on twenty samples of each type to minimize statistical variations. The maximum measured forces at the instant of fracture between the crystal solid-substrate were converted to a measure of the shear strength of CyC5 hydrate adhesion by dividing over the known cross-section area of the ice-substrate interface for each cuvette (1 cm^2).

ASSOCIATED CONTENT

Supporting Information. The video of hydrate formation can be accessed from the Supporting Information. This material is available free of charge via the Internet at http://pubs.acs.org.

AUTHOR INFORMATION

Corresponding Author

*E-mail: kkg@mit.edu (K.K.G.); gareth@mit.edu (G.H.M)

ACKNOWLEDGMENT

The authors gratefully acknowledge support from the Chevron-MIT Energy Initiative program.

REFERENCES

1. Sloan, E. D.; Koh, C. A., *Clathrate Hydrates of Natural Gases*. 2007.
2. Dyadin, Y. A.; Bondaryuk, I. V.; Aladko, L. S., Stoichiometry of clathrates. *Journal of Structural Chemistry* **1995,** *36* (6), 995-1045.
3. Bollavaram, P.; Devarakonda, S.; Selim, M. S.; Sloan, E. D., Growth kinetics of single crystal sII hydrates - Elimination of mass and heat transfer effects. In *Gas Hydrates: Challenges for the Future*, Holder, G. D.; Bishnoi, P. R., Eds. 2000; Vol. 912, pp 533-543.
4. Wilson, P. W.; Lester, D.; Haymet, A. D. J., Heterogeneous nucleation of clathrates from supercooled tetrahydrofuran (THF)/water mixtures, and the effect of an added catalyst. *Chemical Engineering Science* **2005,** *60* (11), 2937-2941.
5. Sum, A. K.; Koh, C. A.; Sloan, E. D., Clathrate Hydrates: From Laboratory Science to Engineering Practice. *Industrial & Engineering Chemistry Research* **2009,** *48* (16), 7457-7465.
6. Aman, Z. M.; Olcott, K.; Pfeiffer, K.; Sloan, E. D.; Sum, A. K.; Koh, C. A., Surfactant Adsorption and Interfacial Tension Investigations on Cyclopentane Hydrate. *Langmuir* **2013,** *29* (8), 2676-2682.
7. Ecker, C.; Dvorkin, J.; Nur, A., Sediments with gas hydrates: Internal structure from seismic AVO. *Geophysics* **1998,** *63* (5), 1659-1669.
8. Gbaruko, B. C.; Igwe, J. C.; Gbaruko, P. N.; Nwokeoma, R. C., Gas hydrates and clathrates: Flow assurance, environmental and economic perspectives and the Nigerian liquified natural gas project. *J. Pet. Sci. Eng.* **2007,** *56* (1-3), 192-198.
9. Devarakonda, S.; Groysman, A.; Myerson, A. S., THF-water hydrate crystallization: an experimental investigation. *Journal of Crystal Growth* **1999,** *204* (4), 525-538.
10. Koh, C. A.; Westacott, R. E.; Zhang, W.; Hirachand, K.; Creek, J. L.; Soper, A. K., Mechanisms of gas hydrate formation and inhibition. *Fluid Phase Equilibria* **2002,** *194*, 143-151.
11. Gao, S. Q., Hydrate Risk Management at High Watercuts with Anti-agglomerant Hydrate Inhibitors. *Energy & Fuels* **2009,** *23*, 2118-2121.
12. Smith, J. D.; Meuler, A. J.; Bralower, H. L.; Venkatesan, R.; Subramanian, S.; Cohen, R. E.; McKinley, G. H.; Varanasi, K. K., Hydrate-phobic surfaces: fundamental studies in clathrate hydrate adhesion reduction. *Physical Chemistry Chemical Physics* **2012,** *14* (17), 6013-6020.
13. Sojoudi, H.; McKinley, G. H.; Gleason, K. K., Linker-Free Grafting of Fluorinated Polymeric Cross-linked Network Bilayers for Durable Reduction of Ice Adhesion. *Materials Horizons* **2014**, DOI: 10.1039/C4MH00162A.
14. Coclite, A. M.; Howden, R. M.; Borrelli, D. C.; Petruczok, C. D.; Yang, R.; Yague, J. L.; Ugur, A.; Chen, N.; Lee, S.; Jo, W. J.; Liu, A. D.; Wang, X. X.; Gleason, K. K., 25th Anniversary Article: CVD Polymers: A New Paradigm for Surface Modification and Device Fabrication. *Adv. Mater.* **2013,** *25* (38), 5392-5422.
15. Coclite, A. M.; Shi, Y. J.; Gleason, K. K., Grafted Crystalline Poly-Perfluoroacrylate Structures for Superhydrophobic and Oleophobic Functional Coatings. *Adv. Mater.* **2012,** *24* (33), 4534-4539.
16. Ozaydin-Ince, G.; Coclite, A. M.; Gleason, K. K., CVD of polymeric thin films: applications in sensors, biotechnology, microelectronics/organic electronics, microfluidics, MEMS, composites and membranes. *Reports on Progress in Physics* **2012,** *75* (1).
17. Coclite, A. M.; Shi, Y. J.; Gleason, K. K., Controlling the Degree of Crystallinity and Preferred Crystallographic Orientation in Poly-Perfluorodecylacrylate Thin Films by Initiated Chemical Vapor Deposition. *Adv. Funct. Mater.* **2012,** *22* (10), 2167-2176.

18. Yague, J. L.; Gleason, K. K., Enhanced Cross-Linked Density by Annealing on Fluorinated Polymers Synthesized via Initiated Chemical Vapor Deposition To Prevent Surface Reconstruction. *Macromolecules* **2013,** *46* (16), 6548-6554.
19. Sojoudi, H.; Gleason, K. K.; McKinley, G. H., Designing Durable Vapor Deposited Surfaces for Reduced Hydrate Adhesion. *Advanced Materials Interfaces* **2014**.
20. Iida, T.; Mori, H.; Mochizuki, T.; Mori, Y. H., Formation and dissociation of clathrate hydrate in stoichiometric tetrahydrofuran-water mixture subjected to one-dimensional cooling or heating. *Chemical Engineering Science* **2001,** *56* (16), 4747-4758.
21. Ohmura, R.; Shigetomi, T.; Mori, Y. H., Formation, growth and dissociation of clathrate hydrate crystals in liquid water in contact with a hydrophobic hydrate-forming liquid. *Journal of Crystal Growth* **1999,** *196* (1), 164-173.
22. Aman, Z. M.; Brown, E. P.; Sloan, E. D.; Sum, A. K.; Koh, C. A., Interfacial mechanisms governing cyclopentane clathrate hydrate adhesion/cohesion. *Physical Chemistry Chemical Physics* **2011,** *13* (44), 19796-19806.
23. Aman, Z. M.; Joshi, S. E.; Sloan, E. D.; Sum, A. K.; Koh, C. A., Micromechanical cohesion force measurements to determine cyclopentane hydrate interfacial properties. *J. Colloid Interface Sci.* **2012,** *376*, 283-288.
24. Aman, Z. M.; Leith, W. J.; Grasso, G. A.; Sloan, E. D.; Sum, A. K.; Koh, C. A., Adhesion Force between Cyclopentane Hydrate and Mineral Surfaces. *Langmuir* **2013,** *29* (50), 15551-15557.
25. Aspenes, G.; Dieker, L. E.; Aman, Z. M.; Hoiland, S.; Sum, A. K.; Koh, C. A.; Sloan, E. D., Adhesion force between cyclopentane hydrates and solid surface materials. *J. Colloid Interface Sci.* **2010,** *343* (2), 529-536.
26. Taylor, C. J.; Dieker, L. E.; Miller, K. T.; Koh, C. A.; Sloan, E. D., Micromechanical adhesion force measurements between tetrahydrofuran hydrate particles. *J. Colloid Interface Sci.* **2007,** *306* (2), 255-261.
27. Dieker, L. E.; Aman, Z. M.; George, N. C.; Sum, A. K.; Sloan, E. D.; Koh, C. A., Micromechanical Adhesion Force Measurements between Hydrate Particles in Hydrocarbon Oils and Their Modifications. *Energy & Fuels* **2009,** *23*, 5966-5971.
28. Yang, S. O.; Kleehammer, D. M.; Huo, Z. X.; Sloan, E. D.; Miller, K. T., Temperature dependence of particle-particle adherence forces in ice and clathrate hydrates. *J. Colloid Interface Sci.* **2004,** *277* (2), 335-341.
29. Song, J. H.; Couzis, A.; Lee, J. W., Direct Measurements of Contact Force between Clathrate Hydrates and Water. *Langmuir* **2010,** *26* (12), 9187-9190.
30. Song, J. H.; Couzis, A.; Lee, J. W., Investigation of Macroscopic Interfacial Dynamics between Clathrate Hydrates and Surfactant Solutions. *Langmuir* **2010,** *26* (23), 18119-18124.
31. Karanjkar, P. U.; Lee, J. W.; Morris, J. F., Calorimetric investigation of cyclopentane hydrate formation in an emulsion. *Chemical Engineering Science* **2012,** *68* (1), 481-491.
32. Karanjkar, P. U.; Lee, J. W.; Morris, J. F., Surfactant Effects on Hydrate Crystallization at the Water-Oil Interface: Hollow-Conical Crystals. *Crystal Growth & Design* **2012,** *12* (8), 3817-3824.
33. Zylyftari, G.; Lee, J. W.; Morris, J. F., Salt effects on thermodynamic and rheological properties of hydrate forming emulsions. *Chemical Engineering Science* **2013,** *95*, 148-160.
34. Nakajima, M.; Ohmura, R.; Mori, Y. H., Clathrate Hydrate Formation from Cyclopentane-in-Water Emulsions. *Industrial & Engineering Chemistry Research* **2008,** *47* (22), 8933-8939.
35. Sefidroodi, H.; Abrahamsen, E.; Kelland, M. A., Investigation into the strength and source of the memory effect for cyclopentane hydrate. *Chemical Engineering Science* **2013,** *87*, 133-140.

36. Brown, C. J.; Ni, X., Evaluation of rate of cyclopentane hydrate formation in an oscillatory baffled column using laser induced fluorescence and energy balance. *Chemical Engineering Journal* **2010,** *157* (1), 131-139.
37. Sojoudi, H.; McKinley, G. H.; Gleason, K. K., Linker-Free Grafting of Flourinated Polymeric Cross-Linked Netwrofk Bilayers for Durable Reduction of Ice Adhesion. *Materials Horizons* **2014**.
38. Ozaydin-Ince, G.; Gleason, K. K., Transition between kinetic and mass transfer regimes in the initiated chemical vapor deposition from ethylene glycol diacrylate. *J. Vac. Sci. Technol. A* **2009,** *27* (5), 1135-1143.
39. Yang, R.; Buonassisi, T.; Gleason, K. K., Organic Vapor Passivation of Silicon at Room Temperature. *Adv. Mater.* **2013,** *25* (14), 2078-2083.
40. Petruczok, C. D.; Yang, R.; Gleason, K. K., Controllable Cross-Linking of Vapor-Deposited Polymer Thin Films and Impact on Material Properties. *Macromolecules* **2013,** *46* (5), 1832-1840.
41. Zhang, Y. F.; Debenedetti, P. G.; Prud'homme, R. K.; Pethica, B. A., Differential scanning calorimetry studies of clathrate hydrate formation. *Journal of Physical Chemistry B* **2004,** *108* (43), 16717-16722.
42. Fouconnier, B.; Komunjer, L.; Ollivon, M.; Lesieur, P.; Keller, G.; Clausse, D., Study of CCl(3)F hydrate formation and dissociation in W/O emulsion by differential scanning calorimetry and X-ray diffraction. *Fluid Phase Equilibria* **2006,** *250* (1-2), 76-82.
43. Clausse, D., Differential thermal analysis, differential scanning calorimetry, and emulsions. *Journal of Thermal Analysis and Calorimetry* **2010,** *101* (3), 1071-1077.
44. Feistel, R.; Wagner, W., A new equation of state for H2O ice Ih. *Journal of Physical and Chemical Reference Data* **2006,** *35* (2), 1021-1047.
45. Smith, G. W.; Sorg, L. V., The measurement of boundary tension by the pendant-drop method. I The aliphatic alcohols. *Journal of Physical Chemistry* **1941,** *45* (4), 671-681.
46. Hennig, A.; Grundke, K.; Frenzel, R.; Stamm, M., Ultrahydrophobic surfaces: Relation between roughness and contact angle hysteresis. *Tenside Surfactants Detergents* **2002,** *39* (6), 243-246.
47. Corak, D.; Barth, T.; Hoiland, S.; Skodvin, T.; Larsen, R.; Skjetne, T., Effect of subcooling and amount of hydrate former on formation of cyclopentane hydrates in brine. *Desalination* **2011,** *278* (1-3), 268-274.
48. De Souza, E. J.; Gao, L. C.; McCarthy, T. J.; Arzt, E.; Crosby, A. J., Effect of contact angle hysteresis on the measurement of capillary forces. *Langmuir* **2008,** *24* (4), 1391-1396.
49. Gao, L. C.; McCarthy, T. J., Teflon is hydrophilic. Comments on definitions of hydrophobic, shear versus tensile hydrophobicity, and wettability characterization. *Langmuir* **2008,** *24* (17), 9183-9188.
50. Gao, L. C.; McCarthy, T. J., Wetting 101 degrees. *Langmuir* **2009,** *25* (24), 14105-14115.
51. Meuler, A. J.; Smith, J. D.; Varanasi, K. K.; Mabry, J. M.; McKinley, G. H.; Cohen, R. E., Relationships between Water Wettability and Ice Adhesion. *Acs Applied Materials & Interfaces 2* (11), 3100-3110.
52. Kim, P.; Wong, T. S.; Alvarenga, J.; Kreder, M. J.; Adorno-Martinez, W. E.; Aizenberg, J., Liquid-Infused Nanostructured Surfaces with Extreme Anti-Ice and Anti-Frost Performance. *ACS Nano* **2012,** *6* (8), 6569-6577.
53. Korhonen, J. T.; Huhtamaki, T.; Ikkala, O.; Ras, R. H. A., Reliable Measurement of the Receding Contact Angle. *Langmuir* **2013,** *29* (12), 3858-3863.
54. Subramanyam, S. B.; Rykaczewski, K.; Varanasi, K. K., Ice Adhesion on Lubricant-Impregnated Textured Surfaces. *Langmuir* **2013,** *29* (44), 13414-13418.

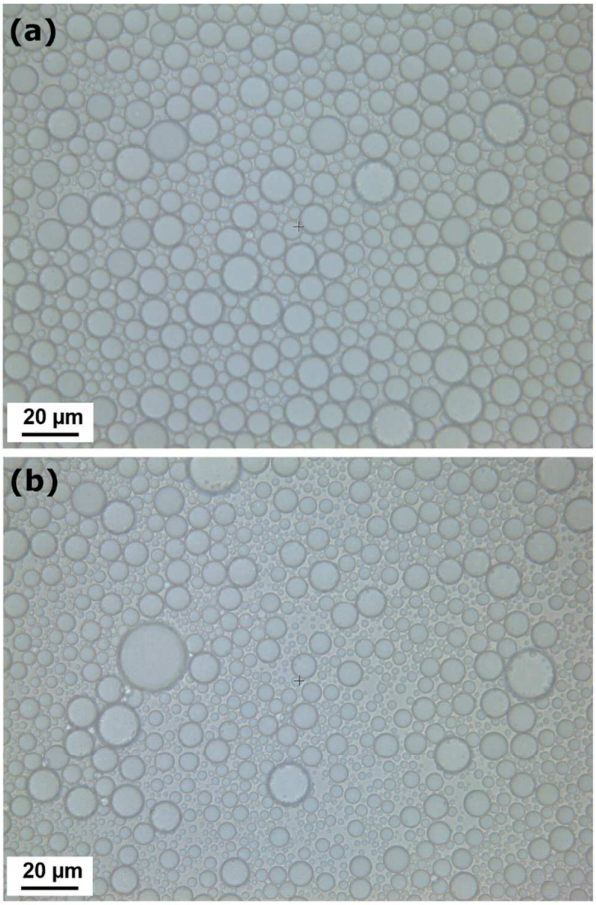

Figure 1. Representative emulsion photomicrographs taken on as-made (top) emulsion and 4 hr after preparation (bottom). Using 10 photomicrographs at each time, the mean droplet diameter was observed to decrease from an ensemble-averaged value of 8.4±3.8 µm to 5.8±3.4 µm after 4 hr. Thus, the emulsions are sufficiently stable to perform hydrate formation experiments by extended cooling.

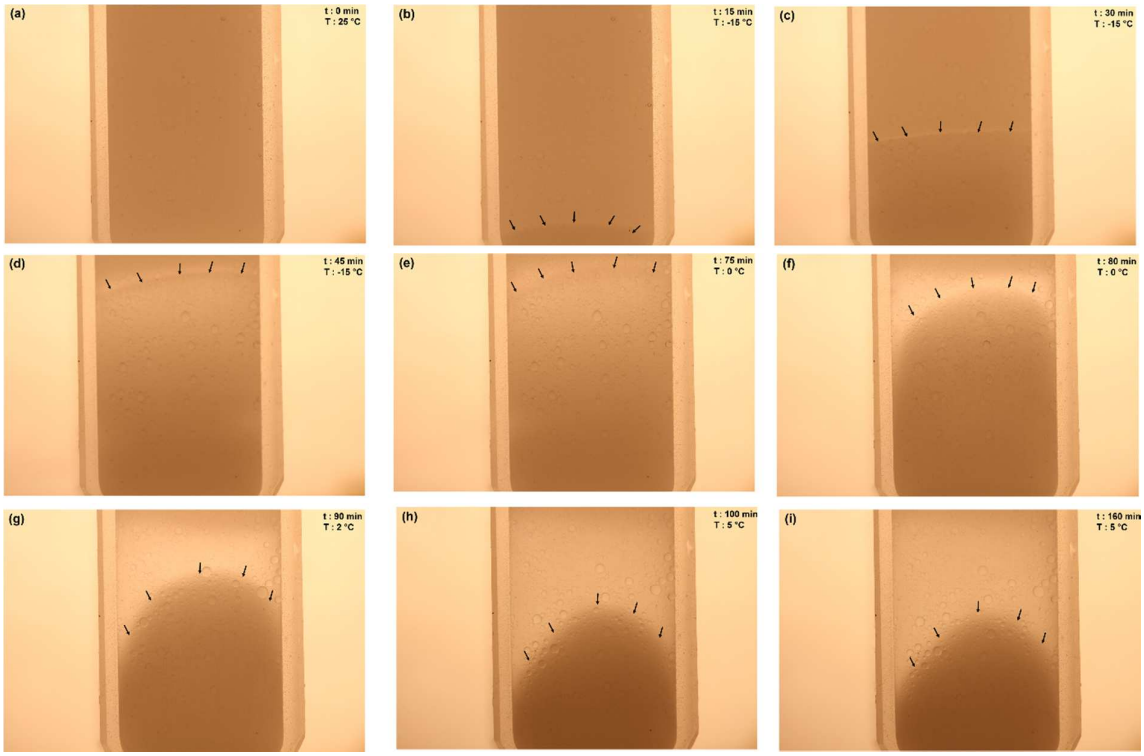

Figure 2. Pictures of cyclopentane hydrate formation from a 17:1 (mole ratio) water:cyclopentane emulsion inside a glass cuvette were taken during visual observation by camera. Arrows indicate the interface of the solid and the emulsion. Video of hydrate formation can be accessed in the Supporting Information. The cross section of the cuvette is 1 cm × 1 cm.

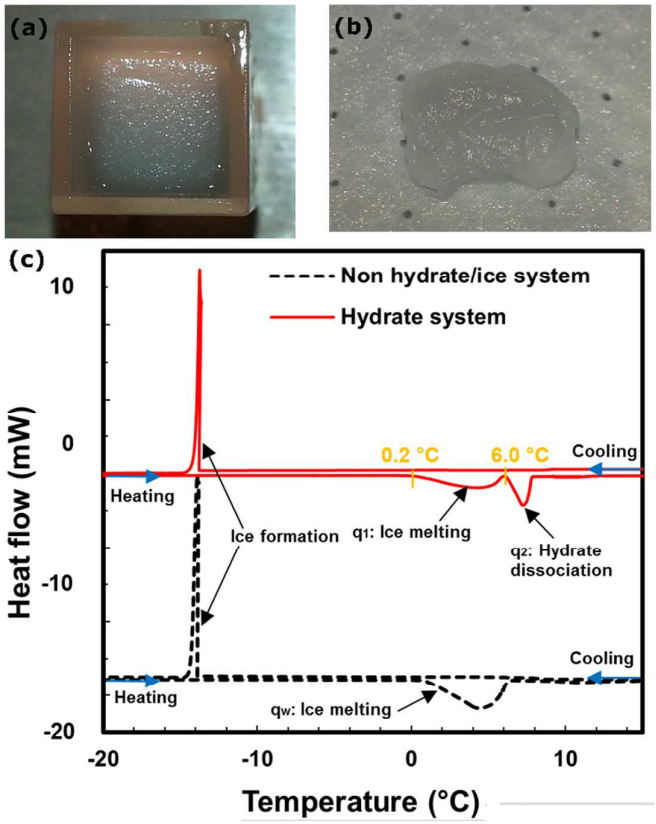

Figure 3. Photographs of (a) the CyC5 hydrate formed inside a cuvette, and (b) a small piece of CyC5 hydrate sampled from the cuvette for the DSC measurements. (c) DSC thermograph of hydrate system (red solid line) and non-hydrate-containing (pure water/ice) system (black dash line). The heating and cooling rates were 1 °C /min. Data for the non-hydrate/ice system is shifted downward for the clarity. The hydrate system shows two separate peaks during heating corresponding to ice melting and hydrate dissociation whereas the non-hydrate/ice system only shows a single ice melting peak.

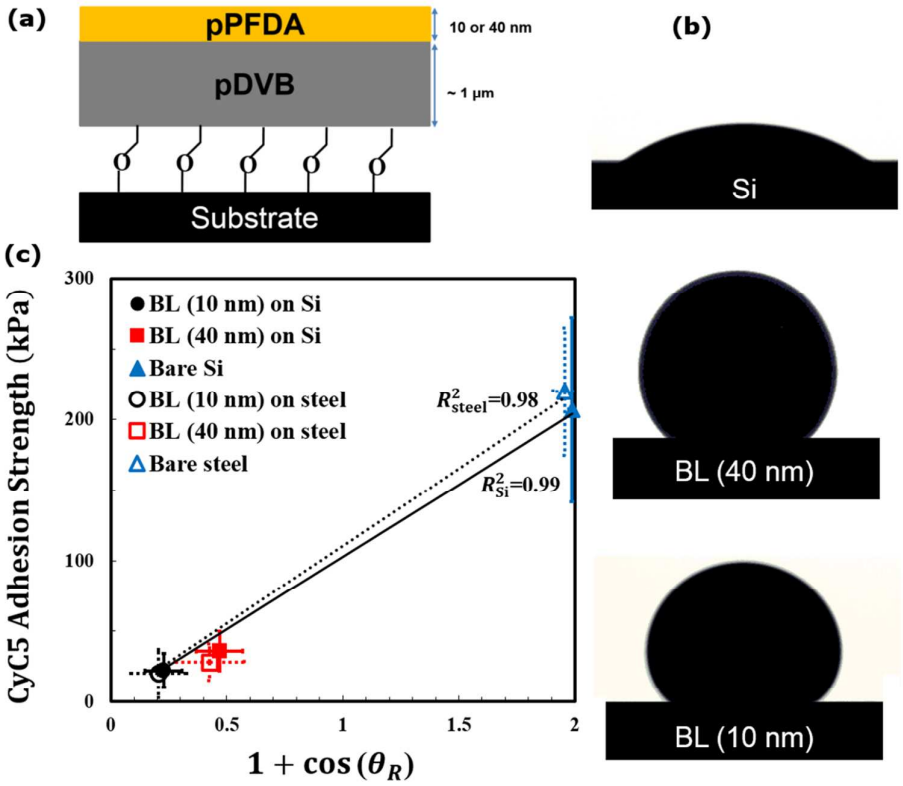

Figure 4. (a) Schematic of the bilayer polymer network deposited on a substrate. (b) Representative images of CyC5-in-water emulsion droplets captured during contact angle measurements on bare Si (top), linker-free grafted bilayer pDVB/pPFDA with 40 nm pPFDA on Si (denoted 'BL (40 nm) on Si') (middle), and linker-free grafted bilayer pDVB/pPFDA with 10 nm pPFDA on Si ('BL (10 nm) on Si') (bottom). (c) Adhesion strength of CyC5 hydrates as a function of the scaled work of adhesion of the CyC5-in-water emulsion on bare and polymer coated substrates. $W^{adh} = \gamma_{LV}(1 + \cos\theta_R)$ where $\gamma_{LV} = 59.3 \pm 1.8$ mN/m. The data suggest that the adhesion strength of the cyclopentane hydrate to the surface correlates well with the work of adhesion of the liquid emulsion used to form the CyC5 hydrates (R^2_{steel} =0.98 and R^2_{Si} =0.99). These data suggest that relatively simple goniometric measurements of CyC5-in-water emulsion droplets can be used as a probe fluid to obtain the work of adhesion and predict the strength of CyC5 hydrates adhesion on a given substrate, which is an extremely challenging experimental measurement.

Table 1. Contact angles for droplets of water and CyC5-in-water emulsion obtained from goniometric measurements on bare Si and steel, and on linker-free grafted bilayers of pDVB/PPFDA. Two bilayer coatings are studied; both consisting of a densely-crosslinked pDVB network and then either (i) a thicker top layer of approximately 40 nm pPFDA deposited on underlying substrates of silicon and steel (denoted `BL (40 nm) on Si' and `BL (40 nm) on steel' respectively), or (ii) a thinner top layer of approximately 10 nm pPFDA on Si and steel (denoted `BL (10 nm) on Si' and `BL (10 nm) on steel'). These data indicate the emulsion-repelling naure of the bilayer polymeric coatings.

	Water Contact Angle		**Emulsion Contact Angle**	
	Receding θ_R^W (°)	**Advancing** θ_A^W (°)	**Receding** θ_R (°)	**Advancing** θ_A (°)
Bare Si	9.6±1.5	32.2±2.8	9.1±1.7	32.5±2.1
BL (40 nm) on Si	132.0±7.8	149.1±1.9	122.1±7.5	135.7±6.7
BL (10 nm) on Si	145.0±1.8	152.0±1.0	140.5±6.6	147.6±5.4
Bare steel	19.9±3.7	76.0±6.5	17.2±3.5	63.1±6.0
BL (40 nm) on steel	143.2±1.7	152.0±2.1	125.2±10.1	138.5±7.5
BL (10 nm) on steel	150.3±1.6	154.2±2.2	142.5±9.8	148.3±4.5

Table 2. Droplet size distribution of hydrate-forming CyC5-in-water emulsion as a function of time.

Time (h)	Mean drop size (μm)	Standard deviation (μm)
0	8.4	3.8
4	5.8	3.4

TOC Graphic

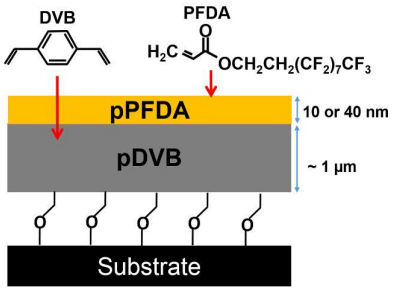
DVB
PFDA
H2C
OCH2CH2(CF2)7CF3
pPFDA
10 or 40 nm
pDVB
~ 1 µm
Substrate